Journal of Metals, Materials and Minerals, 35(1), e2292, 2025

The effect of Fe-NiMnMo high entropy alloy electrode on enhancing the weldability and mechanical properties of railway steel 900A

Sarawut CHAOWAKARNKOOL[1], Kanokwan UTTARASAK[1,2], Sittipong JAIPAYUK[1,2], Narin JANTAPING[1,2], and Man TUIPRAE[1,2,*]

[1] *Department of Industrial Engineering, Faculty of Engineering, Rajamangala University of Technology Lanna, 128 Huay Kaew Road, Muang, Chiang Mai, Thailand, 50300*

[2] *Innovation and Testing of Railway Transportation System Products Research Unit, Center of Excellence in professional and technology, Faculty of Engineering, Rajamangala University of Technology Lanna, 128 Huay Kaew Road, Muang, Chiang Mai, Thailand, 50300*

***Corresponding author e-mail**: tman@rmutl.ac.th

Received date:
21 January 2025
Revised date:
20 February 2025
Accepted date:
10 March 2025

Keywords:
Railway steel 900A;
Fe-NiMnMo electrode;
The flux-cored arc welding (FCAW);
Carbon equivalent (CE);
High entropy alloy

Abstract

The rail transport system is essential for moving passengers and heavy goods over long distances, with steel 900A being a common material used for rail tracks in Thailand. Prolonged exposure to heavy loads and variable environmental conditions can lead to rail track damage known as "engine burn", which results from friction between the train's wheels and the rail. The flux-cored arc welding (FCAW) process is employed to repair these burns due to its use of readily available electrode wires and the efficiency of the repair. However, welding high-carbon steel like rail steel 900A poses challenges, such as a tendency to form martensite in the heat-affected zone and susceptibility to hydrogen cracking. The Fe-NiMnMo electrode has been identified as effective for hard-facing and repairing damaged rail surfaces. This study investigates the efficacy of the FCAW process using Fe-NiMnMo electrodes for repairing engine burns on rail steel 900A. Results demonstrate that the Fe-NiMnMo electrode strongly bonds with rail steel 900A. Multi-pass welding offers superior mechanical properties compared to single-pass welding, showing lower friction coefficients and wear rates. Detailed analysis using X-ray diffraction (XRD), energy dispersive spectroscopy (EDS), Vickers hardness testing, and high-temperature tribometry was studied to assess the mechanical properties and performance of the repaired rails.

1. Introduction

The rail transport system is widely used for moving passengers and heavy cargo, including cement, petroleum, and heavy machinery, over long distances. However, prolonged exposure to heavy loads and varying environmental conditions can lead to damage to the rail tracks. One notable type of damage is engine burn fracture, which develops gradually at the rail head and can ultimately lead to track failure [1]. This failure occurs when the wheels slip on the rail head, generating friction that produces heat on the rail surface and leads to thermal cracking as the rail cools. Such damage can worsen with repeated impacts, wear, and slippage. Welding is an effective repair method due to its efficiency. Fusion welding, a technique that joins metals using a molten pool, includes three primary categories: gas welding, arc welding, and high-energy beam welding [2]. For the railway system, the period between 1910 and 1935 is often considered the golden age of railways. During the mid-1920s, the manual metal-arc welding (MMA) process was introduced as the first method for repairing worn parts in rail crossings [3]. FCAW is an arc welding process primarily used for ferrous metals but is also adaptable for stainless steel, low- and mild-alloy steel, carbon steel, and cast iron, as well as for hard-facing and surface alloys. This process is favoured for its faster welding speeds, lower heat input, and excellent deposition rates, and it can be applied in field conditions. Consequently, many researchers are interested in studying the impact of the FCAW process on the microstructure of rail head surfaces [4,5].

Additionally, it is well known that high carbon content and other alloying elements increase the hardness of steel but reduce its weldability. These properties are linked to the carbon equivalent (CE), which is used to predict the hardenability, weldability, susceptibility to hydrogen-induced cracking, and cracking behaviour in steel [6]. For example, ductility is increased by phosphorus (P) and Sulphur (S). Manganese (Mn) increases hardness. Silicon (Si), copper (Cu), and nitrogen (N) can improve corrosion resistance, while niobium (Nb) and Ni result in an increase in yield strength in steel [7]. The literature on using CE to predict the weldability and preheating requirements of steel is summarized in Table 1.

The most common formula used to calculate carbon equivalent is the American Welding Society (AWS) (Equation (1)) [8]. The carbon equivalent Equation (1) is given as follows:

$$CE = \%C + \frac{\%Mn+\%Si}{6} + \frac{\%Cr+\%Mo+\%V}{5} + \frac{\%Cu+\%Ni}{15} \quad (1)$$

Where CE = carbon equivalent, C = carbon, Mn = manganese, Si = silicon, Cr = chromium, Mo = molybdenum, V = vanadium, Cu = copper, and Ni = nickel.

Moreover, the welding process involves joining different materials between the base metal and filler metal. The dilution rate for each welding process (as shown in Table 2) is used as a multiplying factor to calculate the CE [9]. Thailand's standard rail tracks are made of 900A steel, in accordance with the International Union of Railways standard. The carbon content and trace elements in the 900A rail steel and the filler metal (electrode) are crucial factors affecting the weldability and properties of the welding process. The supplier ensures that Fe-NiMnMo filler metal is well-suited for repairing hard-facing, worn, or damaged surfaces on rails and crossings [10].

This study focuses on the weldability and properties of 900A rail steel weldments using the Fe-NiMnMo electrode with the FCAW process. Optical and scanning electron microscopy (SEM/EDS) were employed to examine the microstructure and relevant phases in the weldment. Crystal structure analysis was performed using X-ray diffraction (XRD), and mechanical properties were assessed using a Vickers hardness tester. Additionally, tribological testing and tribometry were conducted to evaluate the performance of 900A railway steel.

2. Experimental

2.1 Materials and welding procedure

Rail steel grade 900A, with the chemical composition detailed in Table 3 [11], was used as the base metal for the FCAW process. The welding wire employed in this research is the Fe-NiMnMo electrode, a gas-free flux-core wire. This electrode offers excellent metallurgical properties and is perfectly compatible with the base metal, making it ideal for hard-facing wear or repairing rail surface damage. Additionally, this welding wire is specifically designed for use with TRANSLAMATIC robotic welders. The chemical composition of the Fe-NiMnMo electrode, containing a low carbon content of 0.08 wt%, is shown in Table 4. The low carbon content of this welding wire contributes to an excellent dilution ratio of carbon in steel grade 900A, reducing the risk of cracking in the weldment.

Typically, the depth of engine burns on the rail head does not exceed 5 mm. In the FCAW process, the welding layers should be limited to a maximum of two layers. To simulate a worn rail surface, the running surfaces of the base metal were milled and ground to depths of 3 mm and 5 mm. The 3 mm worn surface was welded using the FCAW process for a single-layer weld (Weldment 1), while the 5 mm worn surface was welded with a double-layer application (Weldment 2). The welding parameters used in this experiment are detailed in Table 5.

2.2 Metallurgical examination

Both weldment samples, 1 and 2, were cross-sectioned from the center of the rail track to characterize their microstructural properties. The samples were prepared using conventional metallographic techniques. After polishing, the samples were etched with 2% Nital for 10 sec, following the ASTM E407_99 standard [12]. An optical microscope was used to examine the cross-sections of the base metal, heat-affected zone, and weld metal. Additionally, in-depth microstructural characterization was performed using a Scanning Electron Microscope (TESCAN Model VEGA 3) operating at 20 kV, equipped with SEM/EDS.

Table 1. Carbon equivalent (CE) for weldability and preheating of steel [6-8].

Carbon equivalent (CE)	Weldability	Preheating
Up to 0.35	Excellent	Not Necessary
0.36 to 0.40	Very good	Recommended
0.41 to 0.45	Good	Necessary
0.46 to 0.50	Fair	Necessary
0.51 and over	Poor	Necessary

Table 2. The applied welding process and dilution rate [9].

No.	Applied process	Dilution rate
1.	T.I.G welding	25% to 50%
2.	M.I.G. welding (Spray transfer)	25% to 40%
3.	M.I.G. welding (Dip transfer)	15% to 30%
4.	Metallic-arc welding	25% to 40%
5.	Submerged-arc welding	25% to 50%

Table 3. The chemical composition of the rail steel 900A (UIC 54) [9].

Material	Chemical composition [wt%]							
	C	Si	Mn	P	S	Cr	Ni	Fe
Steel 900A	0.60 - 0.08	0.10 - 0.50	0.80 - 1.30	0.04	0.04	-	-	Bal.

Table 4. The chemical composition of the Fe-NiMnMo electrode [10].

Material	Chemical composition [wt%]									
	C	Si	Mn	P	Si	Cr	Mo	Ni	Al	Fe
TRANSLARAIL Dia. 1.6 mm	0.084	0.821	1.54	0.007	0.0002	0.33	0.59	2.39	1.27	Bal.

Table 5. Parameters for the FCAW processing using the Pluton Arc. 250P CTF, including TRANSLAMATIC 350 controller welding machine.

No.	Parameters	TRANSLARAIL Dia. 1.6 mm
1.	Volt (V)	27
2.	Depth (mm)	3 and 5
3.	Ampere (A)	180
4.	Travel speed for single-layer (cm·min^{-1})	30
5.	Travel speed for double-layer (cm·min^{-1})	30
6.	Temperature before welding (°C)	250
7.	Working distance (mm)	20-25
8.	Welding position	1G
9.	Length of weld line (mm)	15
10.	Type of welding	Automatic

Table 6. Carbon equivalent, which is calculated from the AWS equation multiply with a minimum of 25% dilution for metallic-arc welding process.

Weldment	CE
Calculate from the specification of Rail 900A and Fe-NiMnMo	0.39 to 0.48
Calculate from the chemical composition of base metal and weld metal of weldment 1	0.47
Calculate from the chemical composition of base metal and weld metal of weldment 2	0.44

Table 7. Chemical composition by OES spectrometer of weldment after the FCAW process for single-pass welding.

Area	Run	Chemical composition of weldment 1 (single-layer welding) [wt%]																
		Fe	C	Mn	Si	Cr	V	Co	Cu	Mo	Ni	Al	Ti	Nb	Zn	S	P	N
Rail steel 900A (UIC54)		Bal.	0.60 - 0.80	0.80 - 1.30	0.10 - 0.50	-	-	-	-	-	-	-				0.04	0.007	-
BASE METAL (single-layer)	Run 1	Bal.	0.680	1.382	0.293	0.027	0.004	0.000	0.005	0.008	0.005	0.000	0.002	0.000	0.001	0.001	0.014	0.155
	Run 2	Bal.	0.651	1.227	0.288	0.027	0.003	0.000	0.005	0.008	0.006	0.000	0.002	0.000	0.001	0.000	0.014	0.167
	Run 3	Bal.	0.685	1.227	0.287	0.026	0.003	0.000	0.005	0.008	0.004	0.000	0.002	0.000	0.001	0.001	0.014	0.231
Average		Bal.	0.672	1.279	0.289	0.027	0.003	0.000	0.005	0.008	0.005	0.000	0.002	0.000	0.001	0.001	0.014	0.184
S.D.		-	0.018	0.089	0.003	0.001	0.001	0.000	0.000	0.000	0.001	0.000	0.000	0.000	0.000	0.001	0.000	0.041
WELDING (single-layer)	Run 1	Bal.	0.227	1.490	0.589	0.303	0.006	0.006	0.012	0.399	1.671	0.505	0.002	0.001	0.002	0.000	0.012	0.800
	Run 2	Bal.	0.434	1.270	0.462	0.191	0.003	0.003	0.008	0.235	0.914	0.271	0.002	0.000	0.001	0.000	0.010	0.800
	Run 3	Bal.	0.442	1.493	0.815	0.286	0.006	0.005	0.011	0.376	1.680	0.455	0.004	0.005	0.002	0.000	0.012	0.800
Average		Bal.	0.368	1.418	0.662	0.260	0.005	0.005	0.010	0.337	1.422	0.410	0.003	0.002	0.002	0.000	0.011	0.800
S.D.		-	0.122	0.128	0.179	0.060	0.002	0.002	0.002	0.089	0.440	0.123	0.001	0.003	0.001	0.000	0.001	0.000
Transalarail welding wire		Bal.	0.084	1.54	0.821	0.33	-	-	-	0.590	2.39	1.27	-	-	-	0.0002	0.007	-

Table 8. Chemical composition of weldment by OES spectrometer after FCAW process for multi-pass welding.

Area	Run	Chemical composition of weldment 1 (single-layer welding) [wt.%]																
		Fe	C	Mn	Si	Cr	V	Co	Cu	Mo	Ni	Al	Ti	Nb	Zn	S	P	N
Rail steel 900A (UIC54)		Bal.	0.60 - 0.80	0.80 - 1.30	0.10 - 0.50	-	-	-	-	-	-	-				0.04	0.007	-
BASE METAL (double-layer)	Run 1	Bal.	0.677	1.076	0.263	0.024	0.003	0.000	0.004	0.007	0.005	0.000	0.002	0.000	0.001	0.000	0.014	0.230
	Run 2	Bal.	0.683	1.054	0.261	0.024	0.002	0.000	0.004	0.007	0.005	0.000	0.002	0.000	0.001	0.000	0.012	0.727
	Run 3	Bal.	0.722	1.087	0.266	0.025	0.003	0.000	0.004	0.007	0.006	0.000	0.002	0.000	0.000	0.000	0.014	0.574
Average		Bal.	0.694	1.072	0.263	0.024	0.003	0.000	0.004	0.007	0.005	0.000	0.002	0.000	0.001	0.000	0.013	0.510
S.D.		-	0.024	0.017	0.003	0.001	0.001	0.000	0.000	0.000	0.001	0.000	0.000	0.000	0.001	0.000	0.001	0.255
WELDING (double-layer)	Run 1	Bal.	0.266	1.334	0.936	0.277	0.005	0.005	0.010	0.389	1.383	0.483	0.004	0.005	0.002	0.000	0.010	0.800
	Run 2	Bal.	0.311	1.329	0.820	0.266	0.006	0.005	0.009	0.358	1.640	0.441	0.004	0.004	0.002	0.000	0.010	0.800
	Run 3	Bal.	0.238	1.369	0.647	0.299	0.004	0.006	0.011	0.380	1.696	0.485	0.003	0.002	0.002	0.000	0.010	0.800
Average		Bal.	0.368	0.272	1.344	0.801	0.281	0.005	0.001	0.010	0.376	1.573	0.470	0.004	0.004	0.002	0.000	0.010
S.D.		-	0.122	0.037	0.022	0.145	0.017	0.001	0.001	0.001	0.016	0.167	0.025	0.001	0.002	0.000	0.000	0.000
Transalarail welding wire		Bal.	0.084	0.084	1.54	0.821	0.33	-	-	-	0.590	2.39	1.27	-	-	-	0.0002	0.007

2.3 XRD characterization

The top surface samples of the base metal, heat-affected zone, and weld metal were analyzed using a Rigaku Miniflex Benchtop X-ray Diffractometer. This instrument utilized Cu Kα radiation (λ = 1.54060 Å) and was operated at 40 kV and 15 mA. X-ray diffraction data were collected over a 2θ range of 20° to 110°, with a scan speed of 2.00°·min^{-1} and a step size of 0.01°.

2.4 Tribology analysis

For the tribology analysis, the top surfaces of weld metal samples no. 1 and no. 2 were ground with sandpaper (no. 1000) and then tested using a high-temperature tribometer (CSM INSTRUMENTS) in conjunction with an analytical balance (ADAM EQUIPMENT/ PW254), following ASTM G99 standards. The testing conditions were as follows:

Alumina ball :	6 mm
Radius :	3 mm
Load :	5 N
Linear Distance :	500 m
Speed :	8.5 cm·s^{-1}
Testing temperature :	25°C\

2.5 Microhardness testing

The Vickers hardness tester was employed to measure the hardness across the cross-sections of the welding samples. The initial indentation was made from the base metal to the weld metal. A load of 100 gf (0.98 HV) was used with a dwell time of 10 sec. Indentations were spaced 0.5 mm apart. As a result, the distances from the heat-affected zone to the weld metal were 13.5 mm and 18.5 mm for weldments 1 and 2, respectively.

3. Result and discussion

3.1 Carbon equivalent and weldability

3.1.1 The carbon equivalent calculated from the chemical composition of rail 900A UIC 54 (Table 3) and the supplier's electrode specification (Table 4)

The carbon equivalent of rail 900A, when filled with the Fe-NiMnMo electrode using the FCAW process and factoring in a minimum dilution rate of 25% from metallic-arc welding [9], ranges from 0.39 to 0.48, as shown in Table 6. These values indicate fair to good weldability, suggesting that preheating [6-8] the base metal before welding is necessary. This assessment is an initial step in the electrode selection process.

3.1.2 The carbon equivalent calculated from the chemical composition of the weldment samples (Table 7-8) after the FCAW process with the Fe-NiMnMo.

The carbon equivalent of rail 900A, when using the Fe-NiMnMo electrode in the FCAW process with a minimum dilution rate of 25% from metallic-arc welding [9], is 0.47 and 0.44 for weldments 1 and 2 (Table 6), respectively. These CE values suggest that the Fe-NiMnMo electrode provides good weldability for rail 900A during FCAW. This prediction is supported by the observed complete fusion at the interface between the base metal and weld metal in both weldments 1 and 2, as shown in Figure 1, with no cracking at this interface. Therefore, the Fe-NiMnMo electrode is suitable for effectively repairing rail 900A.

3.2.1 The effect of using Fe-NiMnMo electrode as a welding wire in the FCAW process on the microstructure and hardness properties of the rail steel 900A.

Figure 4 presents the average hardness (HV) measurements on the cross-sectional surface of rail steel 900A for both single-pass and double-pass welding during the FCAW process. These measurements span from the base metal to the weld metal. For single-pass welding (weldment 1), the total average hardness is 299.28 ± 39.3 HV, while for double-pass welding (weldment 2), it is 307.0 ± 38 HV. According to the steel hardness conversion table [19], these correspond to 296 HB and 304 HB for weldments 1 and 2, respectively. Weldment 1's hardness falls within the typical range for rail steel 900A (280 HB to 300 HB), whereas weldment 2's hardness is slightly above this range [20]. This suggests that the Fe-NiMnMo electrode effectively maintains the hardness properties of rail steel after FCAW welding.

In examining the hardness across different zones, the heat-affected zone hardness is 279 ± 20 HV for weldment 1 and 288 ± 33 HV for weldment 2. These values are higher than the base metal due to the heat transfer effects during FCAW. Hardness in the heat-affected zone increases progressively towards the weld metal.

The microstructure of the base metal is pearlitic, consisting of ferrite and cementite phases (Figure. 3(a,b)), consistent with the microstructure of steels used in railroad tracks globally [21,22]. Optical microscopy of the heat-affected zone near the fusion line reveals a light phase at the grain boundaries, resembling iron-carbide (Fe_3C), as shown in Figure 5(a,b). However, Fe_3C is not present in the affected area (Figure 5(c)).

SEM/EDS characterization of the heat-affected zone near the fusion line of weldment 1 is detailed in Figure 6 and Table 9.

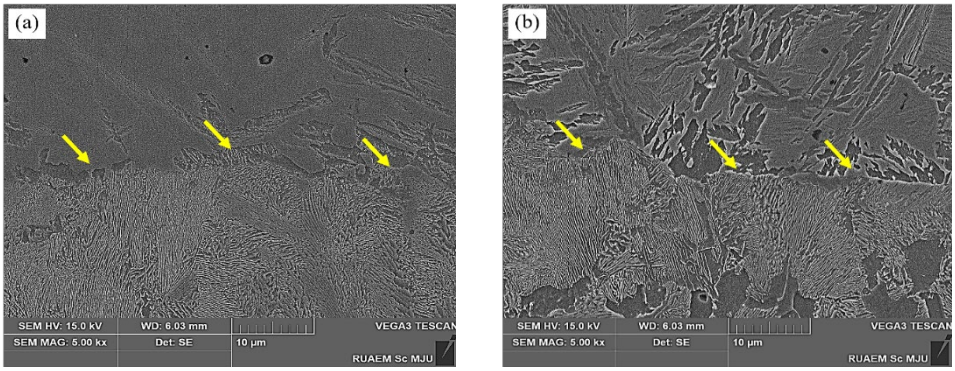

Figure 1. The interface between weld metal and heat-affected zone of (a) weldment 1, and (b) weldment 2.

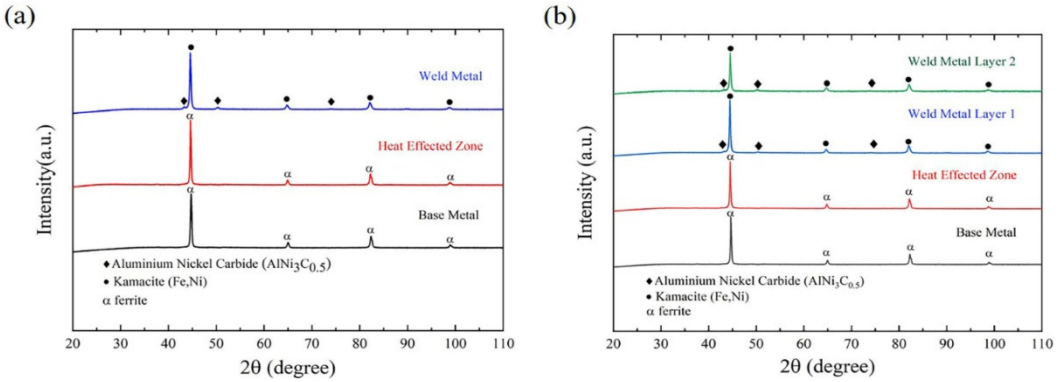

Figure 2. The XRD patterns obtained from the top surface of the rail sample during the FCAW process for single-pass welding (Weldment 1) and multi-pass welding (Weldment 2).

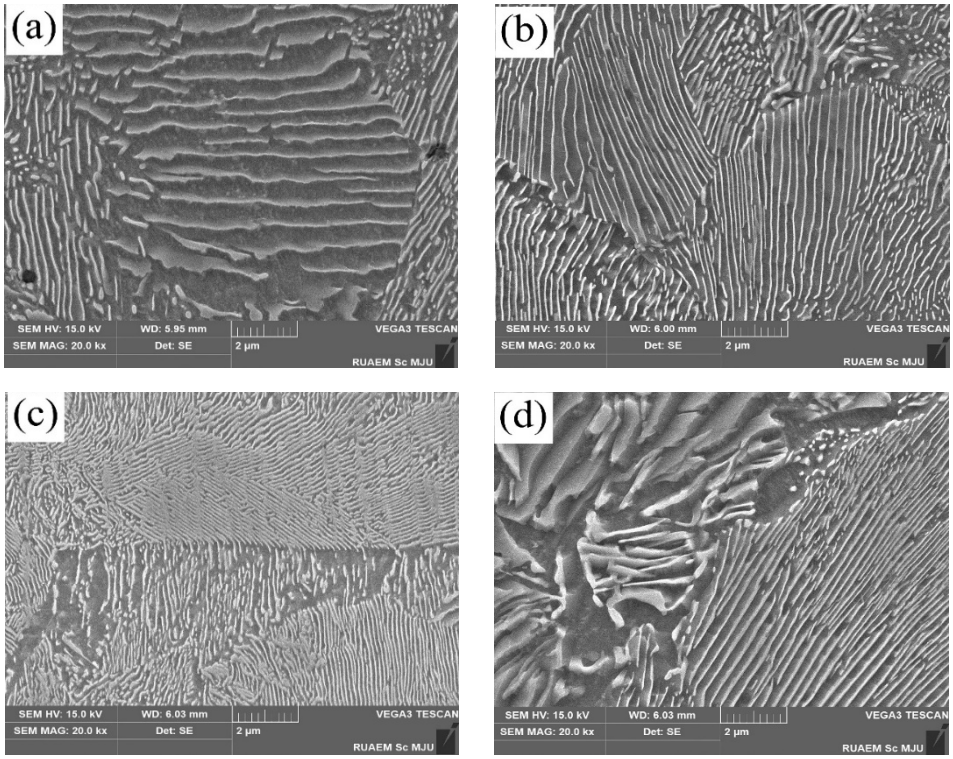

Figure 3. Microstructure of base metal of (a) weldment 1 sample (b) weldment 2 and heat-affected zone of (c) weldment 1 and (d) weldment 2 samples.

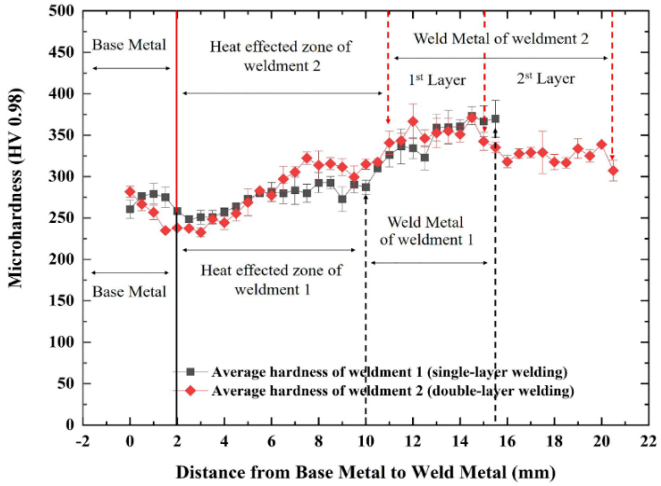

Figure 4. Vicker microhardness testing on the cross-section of weldment samples during the FCAW process.

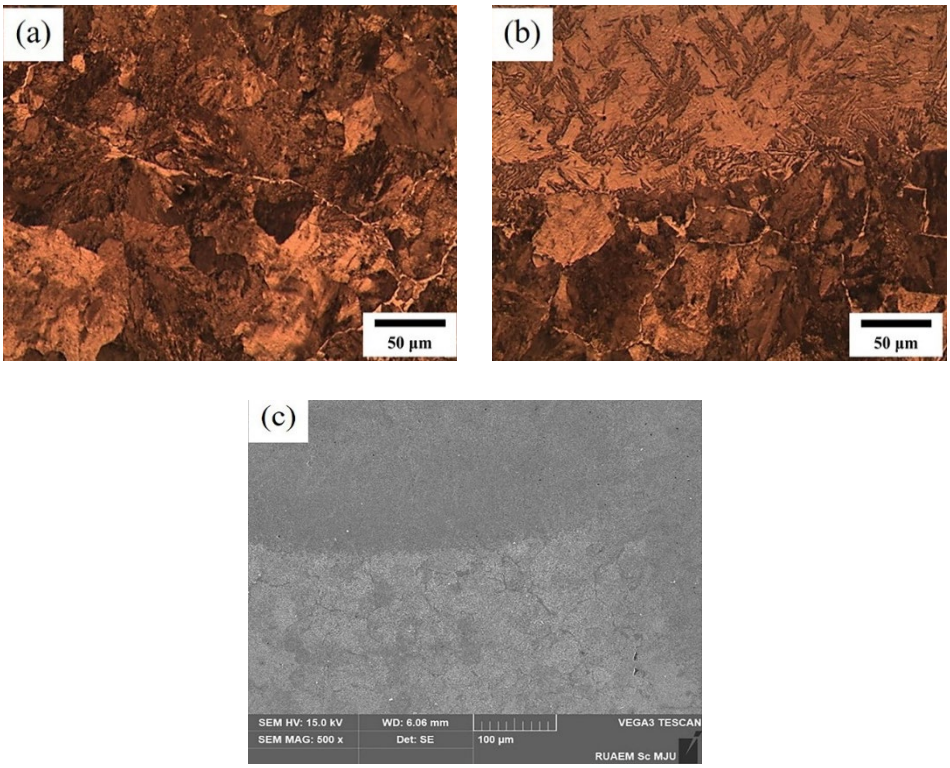

Figure 5. The optical microstructure of weldment 1 sample of (a) the heat-affected zone, (b) the fusion line, and (c) an SEM image of the fusion line.

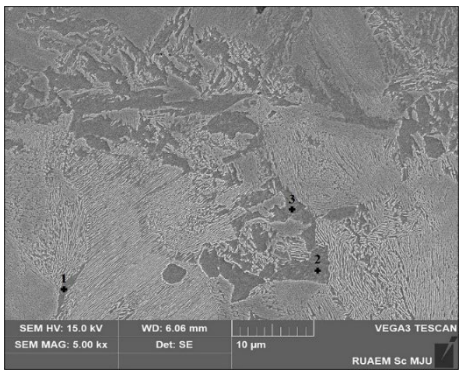

Figure 6. SEM image of point EDS analysis on the heat-affected zone area near the fusion line of weldment 1 sample.

The EDS results indicate the presence of carbon in this area. This suggests that the light phase at the grain boundary is likely pro-eutectoid cementite [16], which contributes to the higher hardness in the heat-affected zone compared to the base metal.

Moreover, the rail steel 900A used in this research contains 0.84 wt% carbon, slightly above the eutectoid composition. The FCAW process operates at temperatures exceeding 725°C, which can influence the microstructure in the heat-affected zone. Consequently, pro-eutectoid cementite [16] typically forms in the heat-affected zone post-welding. Additionally, a small micropore was observed in the weld metal, but there was no cracking at the interface between the heat-affected zone and weld metal (Figure 1(a-b)). Overall, the rail steel 900A and Fe-NiMnMo electrode exhibit a homogeneous and effective weld joint.

In the weld metal area, the hardness values (HV) for both weldment samples 1 and sample 2 are higher than those of the base metal and the heat-affected zone. The average hardness of the weld metal for the first overlayer is 354 ± 6 HV for weldment 1 and 352 ± 12 HV for weldment 2. For the second overlayer, the hardness value of weldment 2 is 324 ± 9 HV.

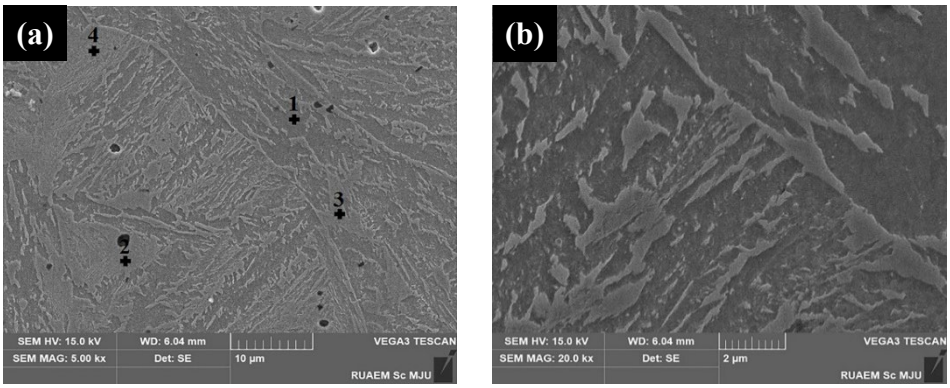

Figure 7. SEM images of weld metal area of weldment 1; (a) EDS point analysis, and (b) SEM mag 20 kX.

The microstructure of the weld metal in weldment 1 is depicted in Figure 7, with the matrix and second phase details provided in Table 10.

The microstructure reveals an irregularly shaped second phase. EDS results in Table 10 indicate that the matrix phase has a lower alloying content compared to the second phase, with carbon preferentially concentrated in the second phase.

For double-layer FCAW welding, the microstructure of weldment 2 is shown in Figure 8. The interface between the heat-affected zone and the first layer of weld metal is well bonded, despite the different materials involved (Figure 8(a-b)). Additionally, the interface between the first and second layers of weld metal is also completely joined (Figure 8(c-d)). EDS results for the second phase in the weld metal, detailed in Table 11, show the presence of C, Mn, Si, Ni, Al, Mo, and Cr. The elements C, Mn, Al, and Cr are known to form carbide phases within the weld metal. This is consistent with the XRD results, which identified the presence of aluminium nickel carbide ($AlNi_3C_{0.5}$) in the weld metal, contributing to the higher hardness observed in this area compared to other regions of the weldment.

3.3 The effect of overlayers on the friction coefficient and wear rate during the FCAW process.

Table 12 summarizes the hardness, friction coefficient (μ), and wear rate of the weld metal for weldment samples 1 and 2 from the flux-cored welding process.

The hardness value of weldment 1 is 354 ± 18 HV, while weldment 2 measures 325 ± 9 HV. Notably, the hardness of weldment 2 is 8% lower than that of weldment 1. Despite this, weldment 2 exhibits a lower friction coefficient (μ) and wear rate compared to weldment 1. This difference may be attributed to the annealing heat treatment that occurred during the double-layer welding of weldment 2.

Table 9. EDS results from the heat-affected zone area near the fusion line of the weldment 1 sample.

EDS Point	Chemical composition [wt%]				
	Fe	C	Mn	Ni	Si
Point 1 (matrix)	94.1	1.6	1.4	1.3	0.6
Point 2 (second phase)	91.4	2.4	1.8	1.7	0.8
Point 3 (second phase)	91.8	2.6	2.1	1.5	0.7
Point 4 (second phase)	93.3	2.4	1.4	1.4	0.4

Table 10. EDS results from the weld metal area of weldment 1.

EDS Point	Chemical composition [wt%]								
	Fe	C	Mn	Ni	Si	Al	Cr	Mo	P
Point 1 (matrix)	94.1	1.6	1.4	1.3	0.6	0.5	0.3	0.2	0.1
Point 2 (second phase)	91.4	2.4	1.8	1.7	0.8	0.4	0.4	1.0	-
Point 3 (second phase)	91.8	2.6	2.1	1.5	0.7	0.4	0.4	0.6	-
Point 4 (second phase)	93.3	2.4	1.4	1.4	0.4	0.6	0.3	0.2	-

Table 11. EDS results from the weld metal area of weldment 2.

EDS point	Chemical composition [wt%]										
	Fe	C	Mn	Si	Ni	Al	Mo	Cr	Ti	P	S
Point 1	96.7	1.8	1.1	0.3	0.1	-	-	-	-	-	-
Point 2	96.1	1.7	1.1	0.4	0.4	0.2	0.1	-	-	-	-
Point 3	96.2	2.2	0.9	0.2	0.2	0.1	-	0.1	-	-	-
Point 4	93.5	2.2	1.4	0.6	1.4	0.5	0.3	0.2	-	-	-
Point 5	92.1	2.5	1.4	0.6	1.8	0.5	0.2	0.3	0.4	-	-
Point 6	93.0	2.2	1.5	0.5	1.5	0.5	0.5	0.2	-	-	-
Point 7	92.8	2.3	1.7	0.7	1.4	0.3	0.4	0.4	-	-	-
Point 8	92.1	4.0	1.1	0.6	1.1	0.7	0.3	0.1	-	-	-
Point 9	91.3	3.0	1.7	0.7	1.7	0.3	0.3	0.2	0.2	-	-
Point 10	94.3	2.2	1.1	0.5	1.2	0.3	0.2	0.3	0.3	-	-
Point 11	93.1	3.0	1.3	0.5	1.2	0.4	0.1	0.2	0.1	-	-
Point 12	93.2	2.3	1.2	0.7	0.7	1.5	0.4	0.2	0.2	-	-
Point 13	92.7	3.1	1.2	0.7	1.5	0.4	0.2	0.2	-	-	-
Point 14	94.4	1.8	1.2	0.5	1.0	0.4	0.4	0.4	-	-	-
Point 15	94.5	1.6	1.5	0.5	1.2	0.4	0.2	0.2	-	-	-
Point 16	92.6	3.7	1.2	0.5	1.1	0.4	0.3	0.2	-	-	-
Point 17	91.5	5.2	1.1	0.5	0.9	0.4	0.2	0.3	-	-	-
Point 18	95.4	-	1.4	0.6	1.4	0.5	0.5	0.2	-	-	-
Point 19	91.0	2.4	1.9	0.9	1.7	0.4	0.9	0.5	-	0.2	0.1
Point 20	92.1	2.7	1.4	0.8	1.7	0.5	0.3	0.4	-	0.1	0.1
Point 21	91.3	3.1	1.6	0.8	1.8	0.5	0.6	0.3	-	0.1	-
Point 22	91.6	3.3	1.5	0.7	1.6	0.5	0.3	0.4	0.1	-	-

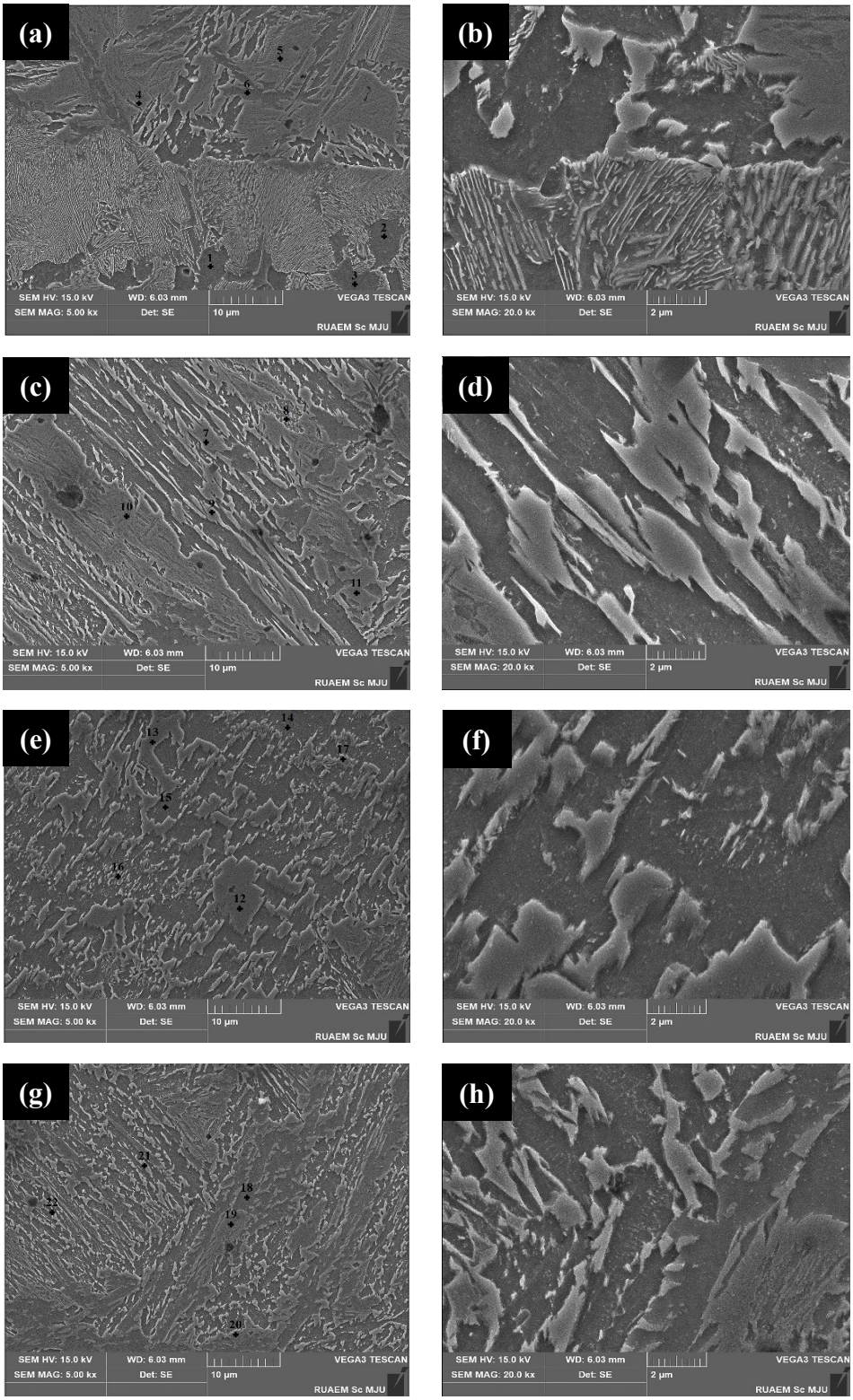

Figure 8. Microstructure of the weldment 2 of (a-b) fusion line, (c-d) the 1st layer of weld metal, (d-e) interface between the 1st layer and 2nd-layer of weld metal, and (f-g) the 2nd layer of welt metal.

Table 12. The hardness (HV), friction coefficient (μ), dis volume loss (mm^3), and wear rate of the weld metal of rail steel 900A samples during flux cored arc welding process.

Sample	Welding	Hardness [HV]	Friction coefficient [μ]	Disk volume loss [mm^3]	Wear rate [$mm^3 \cdot m^{-1}$]
Weldment 1	Single-layer	354 ± 18	0.542	0.01954 ± 0.002	7.81×10^{-6}
Weldment 2	Double-layer	325 ± 9	0.511	0.01602 ± 0.003	6.41×10^{-6}

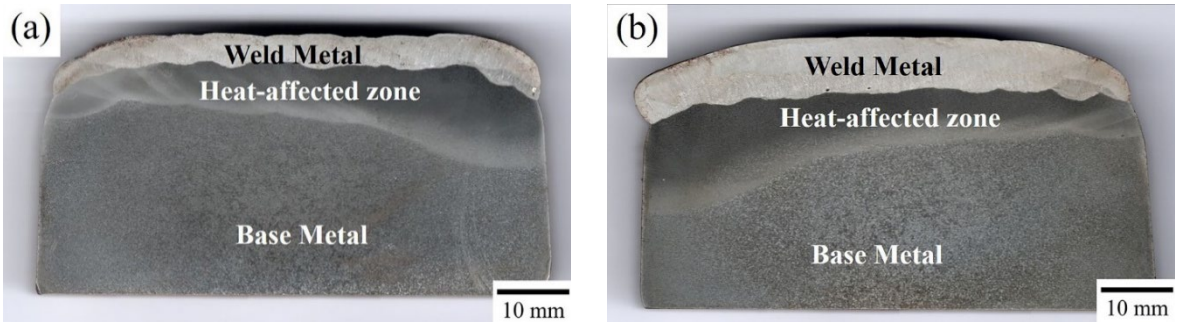

Figure 9. Macrostructure of (a) weldment 1 and (b) weldment 2.

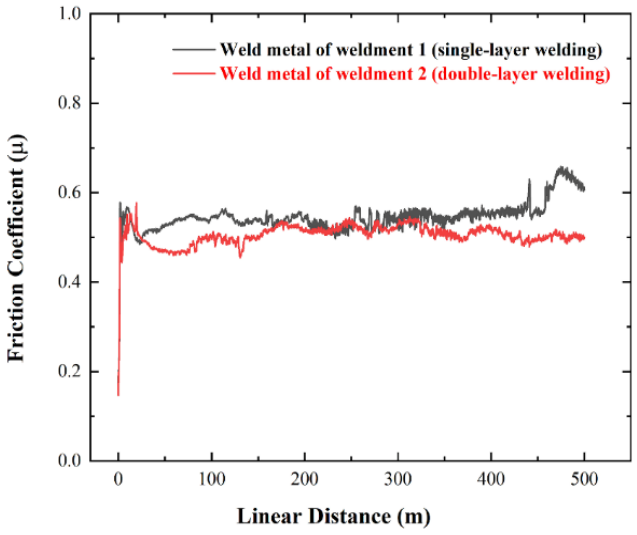

Figure 10. Friction Coefficient (μ) graph from the weld metal during flux cored arc welding process.

Figure 9 shows that the heat-affected zone of weldment 1 is narrower than that of weldment 2. This is likely due to the heat transfer from the first to the second layer during welding, which contributes to the lower hardness observed. The graph of the friction coefficient (μ) for double-layer welding in weldment 2 (Figure 10) shows a lower and smoother profile compared to single-layer welding, correlating with its lower wear rate. Multi-pass welding results in reduced hardness compared to single-pass welding, as the inter-pass temperature during the second layer welding acts as a heat-treatment process. This results in lower hardness and higher ductility, although the hardness remains within standard limits (<300 HV). Thus, multi-pass welding provides better mechanical properties for rail steel 900A compared to single-pass welding.

4. Conclusion

The Fe-NiMnMo electrode is highly effective for repairing rail steel using FCAW processing. It ensures a uniform microstructure without cracks or lamellar tearing, maintains the hardness of the original rail steel, and provides improved mechanical properties. Multi-pass welding with this electrode results in a lower friction coefficient and wear rate, leading to smoother operation of train wheels on the repaired rail.

Acknowledgements

This study is financially supported by the Thailand Science Research and Innovation (TSRI) and National Science Research and Innovation Fund (NSRF) (Fundamental Fund: Grant 2565FF005/2022). This research work was also partially supported by Metal Fabricated Co., Ltd. and Industrial Engineering Department of Rajamangala University of Technology Lanna.

References

[1] J. B. Akers, "Rail failures resulting from engine wheel burns, including effect of repairing such burns by oxyacetylene or electric welding" *American Railway Engineering Association*, vol.53, pp 894-898, 1952.

[2] S. Kou, Welding Metallurgy. 2nd ed. New Jersey: A John Wiley & Sond, Inc., 2002.

[3] B. Dahl, and B. Mogard, Repair of the rails on site by welding. Göthenburg: The ESAB group.

[4] M. N. Saiful Akmal, and M. N. Wahab, "Characterization of UIC-54 rail head surface welded by hardfacing using flux-cored steel wire" In M. N Osman Zahid A. S. Abdul Sani, M. R. Mohamad Yasin, Z. Ismail, N. A. Che Lah, and F, Mohd, "Recent trends in manufacturing and materials towards industry 4.0, lecture notes in mechanical engineering", Springer, Singapore, pp. 763-775, 2021.

[5] H. Z. Oo, and P. Muangjunburee, "Improving microstructure and hardness of softening area at HAZ of thermite welding on rail running surface," *Materials Today communications*, vol. 34, 10438, 2023.

[6] M. Alhassan, and Y. Bashiru, "Carbon equivalent fundamentals in evaluating the weldability of microalloy and low alloys steels," *World Journal of Engineering and Technology*, vol. 9, pp. 782-792, 2021.

[7] T. Kasuya, and N. Yurioka, "Carbon equivalent and multiplying factor for hardenability of steel," *Weld Journal*, vol. 72, pp. 263-268, 1993.

[8] J. C. Lippold, Welding metallurgy and weldability. 1st ed., John Wiley & Sons, Inc or related company, 2014.

[9] Amarine Blog, Jan. 2024, "Weld carbon steel to stainless steel," Amarin Blog. [Online]. Available:https://amarineblog.com/2019/05/31/stainless-steel-to-carbon-steel/.

[10] CTF France Sauron. *WPS welding procedure specification for translarail*. Bondoufle Cedex France.

[11] American National Standard, Recommended Practices for the Welding of Rails and Related Rail Components for Use by Rail Vehicles, AWS D15.2/D15.2M, 2013.

[12] Standard practice for micro etching metals and alloys, ASTM E407-99, ASTM International, 1995.

[13] Standard Test Method for Wear Testing with a Pin-on-Disk Apparatus, ASTM G 99-95a, ASTM International , 2000.

[14] P. Muangjunburee, N. Poolsiri, S. Chaideesungnoen, A. Naultem, HZ Oo, and M. Kongpuang , "XRD observation on the weld metal of resurfaced rail steel," *ChiangMai Journal of Science*, vol. 50, no. 4, pp. 1-11, 2023.

[15] O. Crisanand, and A. D Crisan, "Phase transformation and exchange bias effects in mechanically alloyed Fe/magnetite powders," *Journal of Alloys and Compounds*, vol. 509, pp. 6522-6527, 2011.

[16] K. Kiraga, E. Szychta, and L. Szychta L, "Determination of rail steel's phase composition by mean of X-ray diffraction analysis," *Institute of Electrical and Electronics Engineers*, pp. 316-318, 2012.

[17] L. Keller, J. Rask, P. Buseck, Arizona State University, Tempe, Arizona, USA., ICDD Grant-in-Aid, (1986)

[18] D. Smith Penn State University, University Park, Pennsylvania, USA., ICDD Grant-in-Aid, (1976)

[19] Steel Express Limited. "Steel hardness conversion table," [Online]. Available:https://www.steelexpress.co.uk/steel-hardness conversion.html

[20] H. Boer, and H. Masumoto, "Niobium in rail steel," Proceedings of the International Symposium Niobium, Orlando, USA, pp. 1-24, 2001.

[21] R. R. Porcaro, G. L. Faria, L. B. Godefroid, G. R. Apolonio, L. C. Candido, and E. S. J. Pinto, "Microstructure and mechanical properties of a flash butt welded pearlitic rail," *Journal of materials processing technology*, vol. 270, pp. 20-27, 2019.

[22] E. Pereloma, and D. V. Edmonds, Phase transformation in steels: Fundamentals and diffusion-Controlled Transformations. Woodhead Publishing Limited, 2012.